Polymers & biopolymers

Effects of nanocrystallization on surface migration of polypropylene/slip agent composites in accelerated aging

Jong Sung Won[1], Jae Min Lee[2], Pil Gyu Lee[2], Hyeong Yeol Choi[3], Tae Joon Kwak[4,*] , and Seung Goo Lee[2,*]

[1] Robert Frederick Smith School of Chemical and Biomolecular Engineering, Cornell University, Ithaca, NY 14853, USA

[2] Department of Advanced Organic Materials and Textile System Engineering, Chungnam National University, Daejeon 34134, Republic of Korea

[3] Department of Fashion Design, Dong-A University, Busan 49315, Republic of Korea

[4] Center for Systems Biology, Massachusetts General Hospital, Boston, MA 02114, USA

ABSTRACT

The accelerated thermal aging of plastics causes the migration of additives onto specimen surfaces. This is commonly called the "blooming" or "whitening" phenomenon and has long been an issue in the automotive applications of thermoplastic composites. Still, there is a lack of scientific reports regarding crystallization behavior to our best knowledge. This study investigates the mechanism and characteristics of slip agent migration onto injection-molded composite surfaces depending on the behavior of nanocrystallization with thermal aging and develops a method to evaluate the correlation between the internal and external crystallization size and migration of the composites. Slip agent migration was investigated by increasing the spherulite size of PP/slip agent composites, as measured by X-ray diffraction analysis at different periods. It was found that as the crystalline area increased, the low molecular weight slip agents present in the amorphous region migrated to the specimen surface owing to the absence of interactions with the polymer. In addition, surface elemental analysis, lightness, and roughness confirmed that the slip agents migrated to the surface in accelerated thermal aging conditions. The findings of this work provide a better understanding of the correlation between thermal aging and the migration phenomenon of slip agents on the surfaces of thermoplastic composites.

 Springer

GRAPHICAL ABSTRACT
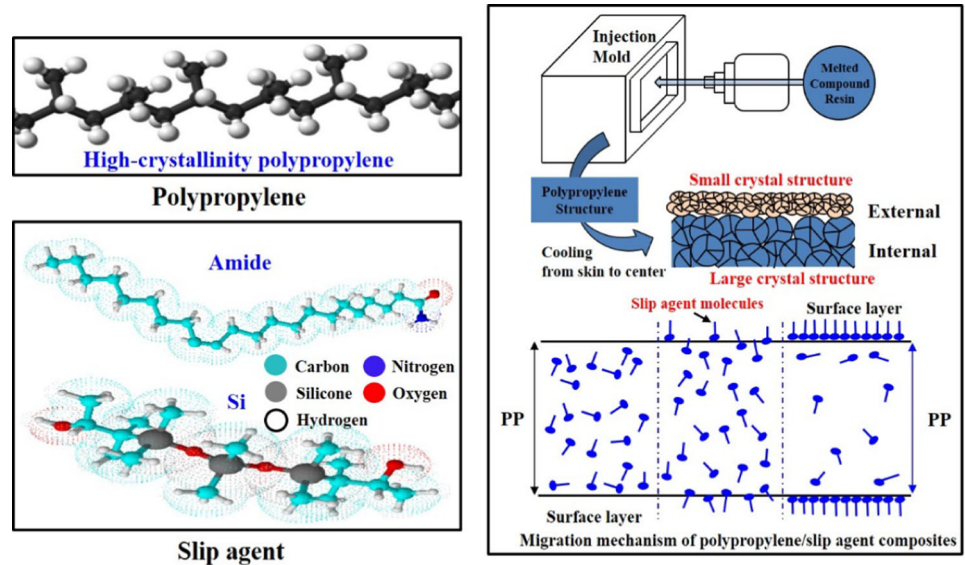
Introduction

Polypropylene (PP) is the most commonly used material for interior automotive components owing to its many advantages, such as being lightweight, low cost, heat resistant, and easy to process. Most PPs are used in many automotive parts, including instrumental panels, bumper fasciae, and door trims, which require the improvement of the functionalities and mechanical properties of nanoadditives [1–3]. Various nanoadditives, such as slip agents, lubricants, antistatic agents, antioxidants, and ultraviolet stabilizers, are added to achieve superior performance of the final products depending on the application [4, 5]. Nanoadditives can significantly improve the mechanical and chemical properties of polymers, such as tensile strength, impact strength, flexibility, elasticity, heat resistance, and dimensional stability of polymers [6–8]. In particular, the friction level between the polymer plastic and equipment is a crucial factor that determines the manufacturing performance. This property is mainly controlled by the coefficient of friction of the plastic. Polymer composites tend to stick to metals and other components of handling lines during fabrication and use. To avoid the demolding of the polymer plastic from the

mold in the process line, the polymer composite material must provide a minimum level of friction [9, 10]. The required coefficient of friction for the composites is commonly achieved using slip agent nanoadditives. These nanoadditives are added to the polymer matrix in the molten stage; they then migrate to the polymer surface in the solid state because of the lack of compatibility between the slip agent and polymeric matrix [11, 12]. Fillers made of talc, mica, silica, and wollastonite are the most common mineral nanoadditives used for polymeric compounds; their content usually ranges from 1 to 40% by weight. Talc, which is a naturally hydrated magnesium silicate, is applied extensively to modify polymeric matrices owing to its various advantages [13]. In particular, talc is cost-effective, improves the stiffness and thermal properties, has a nucleating effect, reduces shrinkage, and imparts dimensional stability. Therefore, talc has been used in final automotive products, such as the interior and exterior parts [14, 15].

Polymer composites with slip agents and talc are not always easy to control because of the multiple factors that influence the migration of the nanoadditive. The migration is most commonly affected by environmental and formulation factors [16, 17]; moreover, the nanoadditive frequently diffuses with
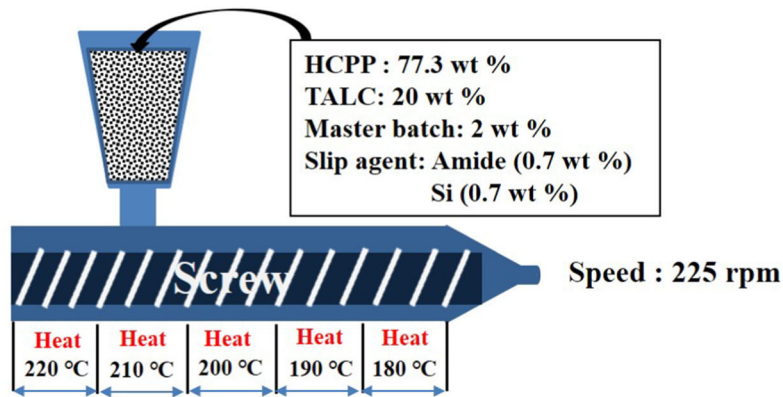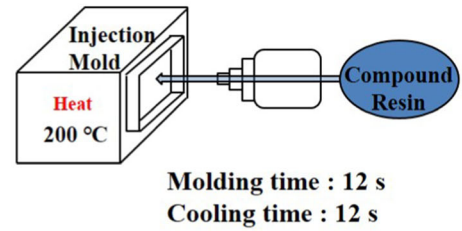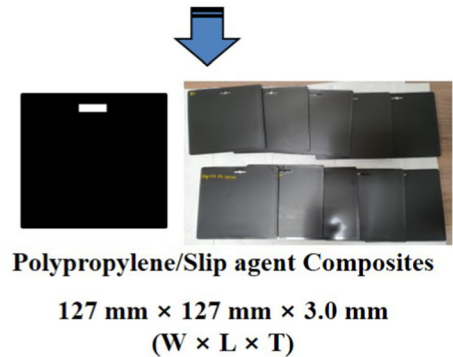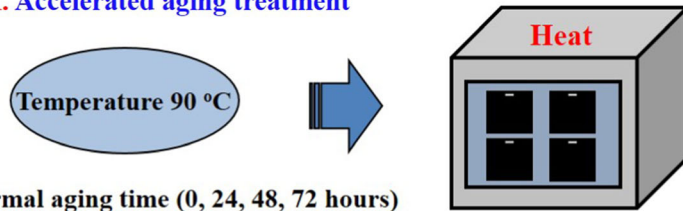
Figure 1 Schematic procedure of surface migration analysis of PP/slip agent composites by thermal aging.

time on the surfaces of the specimens after the extrusion and injection processes, which lead to the phenomenon of "blooming" or "whitening" [18]. The "blooming" of nanoadditive on the surfaces of specimens is a serious issue because it changes the appearance of the final product and also reduces the nanoadditive's function [19]. Such blooming and migration phenomena can be attributed to the influence of the crystallization of the polymer. In a polymer, low molecular weight nanoadditives are present in particularly mobile, amorphous fractions. In the matrix, amorphous fractions may exist between the lamellar stacks in the intraspherulitic zones or at the spherulite borders in the amorphous interspherulitic domains. These fractions act as links between the lamellar stacks in these regions. However, the amorphous fractions undergo changes with thermal aging, which is an outcome attributed to the increase in the density of crystalline fractions owing to an increase in the spherulite size [20]. This changes the mobile part to a partially constrained part owing to thermal aging. The segments of the mobile parts are entangled with each other and cause restricted motion. Kapur and Rogers proposed a molecular rearrangement between the intercrystalline parts in a manner similar to secondary crystallization, thus

suggesting a decrease in the density of the remaining mobile regions [21, 22]. In "secondary crystallization," the penetration of the chains within the adjacent crystals causes the thickening of lamellae and the increase in the crystallite size during thermal aging [23, 24]. Thus, the crystallite size of the specimen gradually increased over time, which may trigger the migration of the nanoadditive to the surfaces of the specimen. However, to our best knowledge, the theoretical interpretation of the blooming phenomenon of nanoadditives has not been reported [25–27]. In addition, most of the published manuscripts only report migration to food packaging materials depending on the aging temperature, molecular weight, and rheological properties of the polymer [28–30]. Experimental evaluation methods and non-standardized test methods need to be developed to study this phenomenon. This evaluation method can improve the quality and life cycle of all thermoplastic composites and PP composites by identifying the migration phenomenon of nanoadditives.

The aim of this study was to investigate the migration of amide and Si as slip agents controlled by co-nanoadditives when incorporated in standard film formulations of PP. The investigation focuses on the relationship between the nanocrystallization

behavior with temperature and time, and the surface migration of the nanoadditive to the internal amorphous regions. The experimental results indicate that the nanoadditive may diffuse out of the surface; they also indicate the correlation between the nanocrystallization behavior and migration phenomena of the nanoadditive on the surface during thermal aging.

Experimental

Materials

Polypropylene (PP) in the form of chips with a melt flow index (MI) of 30 g/10 min (Bx3800, SK Chemicals, Seoul, Seoul, Republic of Korea) was used as the polymer matrix. The following nanoadditives were incorporated in the PP. Armoslip-E (AkzoNobel, Amsterdam, Netherlands) and MO50-001 (Dow Corning, Midland, USA) were used as slip agents.

Preparation of PP/Slip agent composite

Figure 1 illustrates the schematic of the preparation of PP/slip agent composites and the procedure used for the surface migration analysis of the composites subjected to thermal aging. Prior to the extrusion, PP and slip agents were dried in an oven for 3 h at 70 °C. The extrusion of PP/slip agent composites were conducted with the use of a co-rotating twin-screw extruder (TEK20, SM Platek, Ansan, Republic of

Korea, see Fig. S1 for pictures of the machine) with an L/D value of 42 and an intermeshing screw configuration. The screw speed was set to 225 revolutions per minute. The processing temperature was set in the range of 180–220 °C. Further, the PP/slip agent composites were prepared by mixing master batches with the slip agent (amide or Si) at loadings equal to 0.7 wt.%. The extrudates were pelletized using a SM Platek pelletizer. Subsequently, PP/slip agent blend test specimens were prepared using injection molding (IDE140ENII, Goldstar, Seoul, Republic of Korea). To illustrate the diffusion of the internal nanoadditive to the surface over time under annealing conditions, we prepared specimens (thickness = 3 mm) by injection molding. Since the size of the particles varies according to the crystal temperature, the molding and cooling time were fixed as 12 s, respectively, for all cases. The specimens were placed in an oven at 90 °C and annealed for 0, 24, 48, and 72 h. The specimens were split in half at each temperature to examine the nanoadditive migration. The experiments were conducted based on the assumption that the internal nanoadditive diffused outward under thermal aging conditions. Thus, the changes in the specimen surface were identified.

Characterization of PP/Slip agent composite

X-ray diffraction (XRD) analysis was performed at 25 °C using a Bruker AXS D8 diffractometer with a
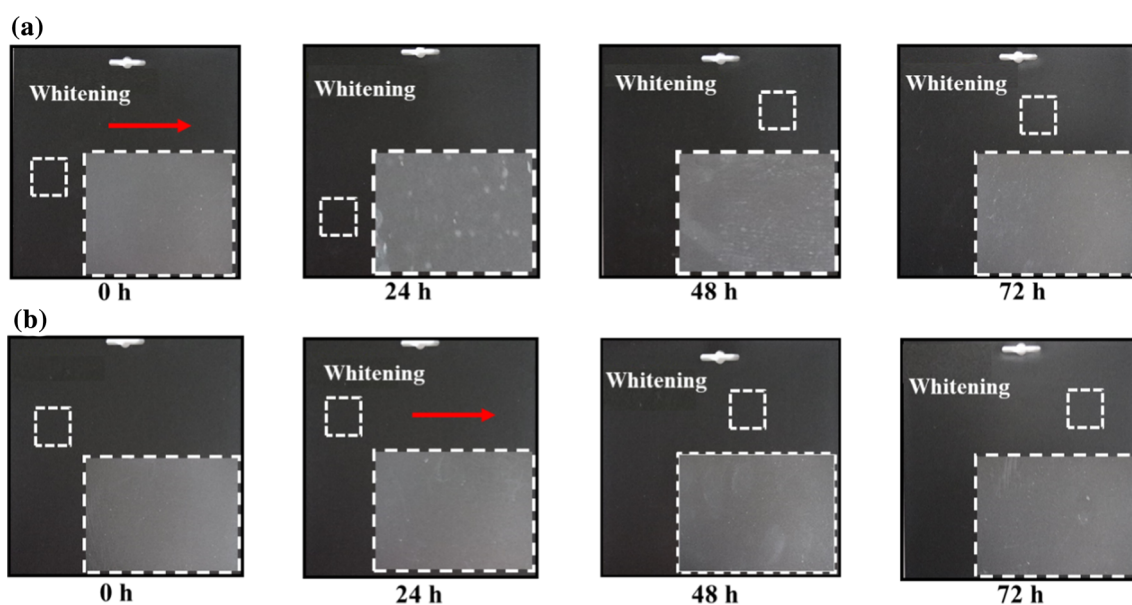

Figure 2 Close-up distal images of **a** PP/amide slip agent and **b** PP/Si slip agent composites aged at 90 °C at different time points.

Cu-tube target (1.541 Å) in standard continuous scan mode. The equipment was operated at 40 kV and 40 mA. The scanning speed was 2.000°/min, and the 2θ range was 5–80°. The measurements were taken on samples with dimensions of 12.7 × 12.7 × 3 mm3. The Origin software was used to obtain the values and figures based on theoretical diffraction patterns.

The Scherrer equation, which is normally used to calculate the nanocrystallite size of crystalline materials, is as follows [31–33],

$$LC = \frac{180}{\pi} \frac{K\lambda}{\cos\theta\sqrt{(FWHM)^2 - s^2}} \qquad (1)$$

where λ is the X-ray wavelength (nm), K is a constant related to a dimensionless shape factor, full width at half maximum (FWHM) is the line broadening at half the maximum intensity of a unit cell, θ is the wavelength of the radiation constant related to a dimensionless shape factor, and the conversion factor 180/π is used to obtain the FWHM value in radians. The thermal characteristics of the compound specimens were measured using a Pyris-1 differential scanning calorimetry (DSC, PerkinElmer, Waltham, USA) instrument. For all tests, 5 mg of each specimen was heated from 25 °C to 200 °C at a rate of 10 °C/min,

held at 200 °C for 10 min, and then cooled to 25 °C at the same rate in a nitrogen atmosphere. DSC analysis is usually performed to determine the degree of crystallinity of a polymer based on the quantification of heat related to its melting. The thermal characteristics of the polymer melt can affect its crystallization behavior. The degree of crystallization was measured from the onset of melting to the end of crystallization, which was determined by the area under the endotherm. The degree of crystallinity was calculated as follows [34].

$$X_c = \frac{\Delta H_m}{\Delta H_{100\%}} \qquad (2)$$

where ΔH_m is the measured melting enthalpy of the samples and $\Delta H_{100\%}$ is the melting enthalpy of 100% crystalline PP, which is approximately 207 J/g [35]. The surface chemical compositions of the PP/slip agent composites were analyzed using an X-ray photoelectron spectrometer (XPS, Multilab 2000, Thermo Fisher Scientific, Waltham, USA). The XPS profiles were obtained using Al Kα (hν = 1400 eV) radiation as the monochromatic X-ray source at an operating voltage of 12 kV. The diamond scratch resistance of the PP/slip agent composites was determined using an Erichsen tester 430 P-II

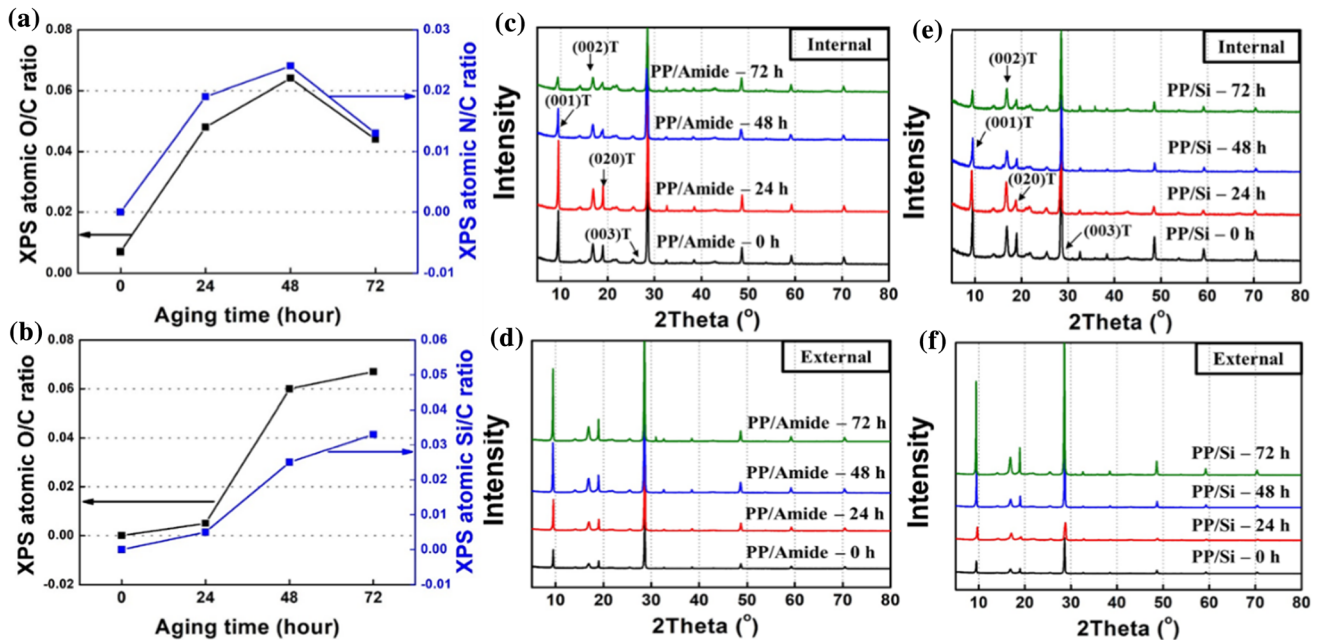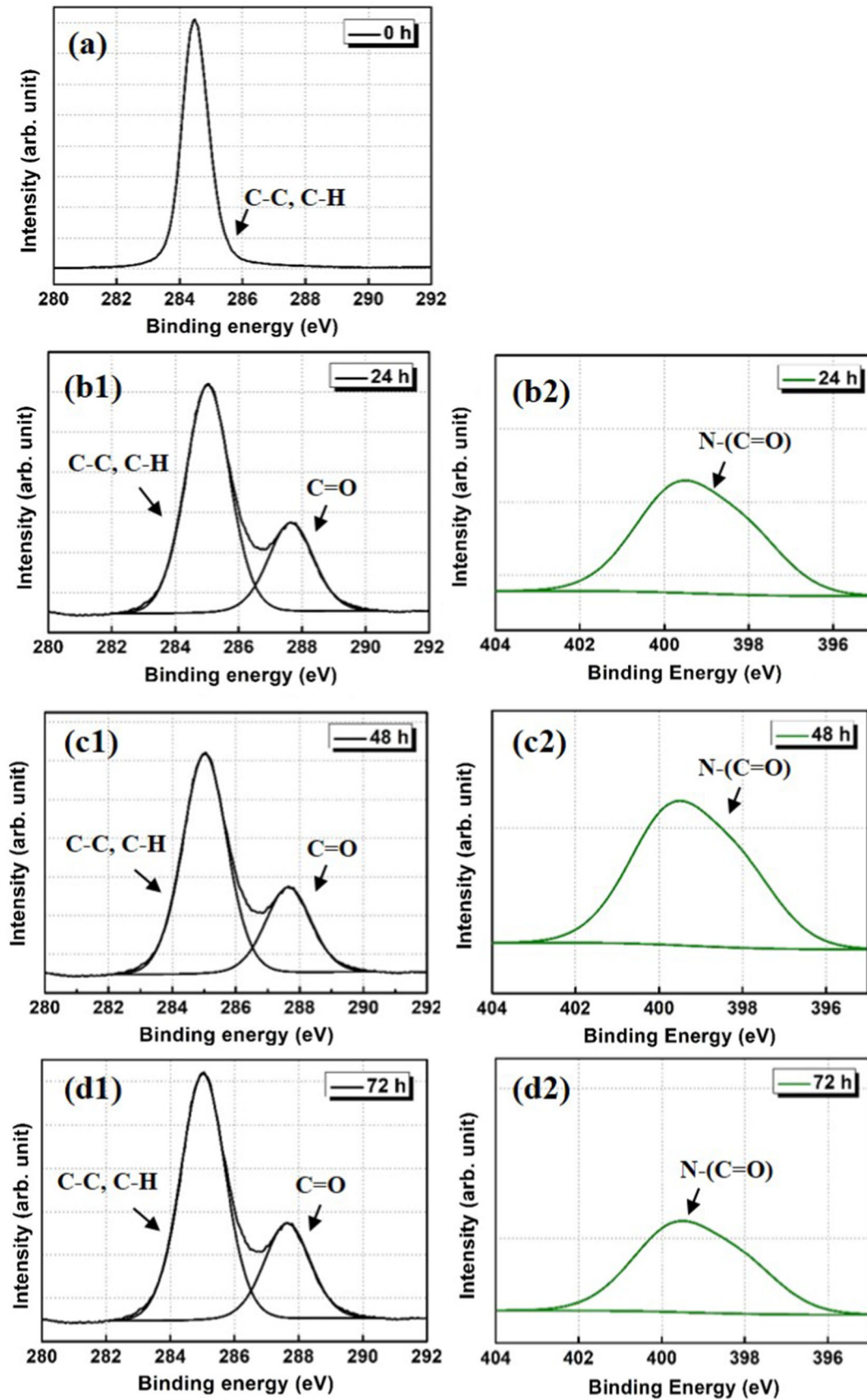**Figure 3** **a** X-ray photoelectron spectroscopy (XPS) atomic ratio of polypropylene (PP) composites with amide slip agent and **b** PP composites with Si slip agent. **c** XRD profiles of internal region and **d** external region of PP/amide composites aged at 90 °C at different times. **e** X-ray diffraction (XRD) profiles of internal region and **f** external region of PP/Si composites aged at 90 °C at different times.

◀**Figure 4** X-ray photoelectron spectroscopy (XPS) C_{1s} and N_{1s} spectra of PP/amide composites aged at 90 °C at different times. **a** C_{1s} spectra, aging time: 0 h, **b** C_{1s} and N_{1s} spectra, aging time: 24 h, **c** C_{1s} and N_{1s} spectra, aging time: 48 h, and **d** C_{1s} and N_{1s} spectra, aging time: 72 h.

(Erichsen GmbH, Germany) according to the American Society for Testing and Materials (ASTM)/ISO polymer scratch standard. Measurements were taken using a force of 10 N. The diameter of the scratch tip was 1 mm. The scratch test was conducted at a speed of 100 mm/s. After the PP/slip agent composites were scratched, the brightness increase of the PP/slip agent composite scratched area was measured using a 6836 spectroguide sphere gloss colorimeter (BYK-Gardner, Wesel, Germany). Subsequently, the brightness difference between the scratched and nonscratched surfaces, delta-L, was determined, and this was used to calculate the brightness deviation. After each scratch, the average surface roughness (Ra) was measured using a surface roughness tester TR200 (SaluTron GmbH, Frechen, Germany). The parameter Ra is generally defined on the basis of the ISO 4287 as the arithmetical mean of the deviations of the roughness profile from the central line (um) along the measurement. This definition is given by Eq. (3) [36],

$$R_a = \frac{1}{L} \int_0^L |y(x)| dx \tag{3}$$

where L is the sampling length, and y is the coordinate of the profile curve. The surface morphological features of the PP/slip agent composites were characterized using a digital camera (IFS-28, Canon). The morphologies of the PP/slip agent composites were analyzed using FESEM (S-4800, Hitachi) equipped with an EDS module. Scratch whitening and structural features of PP/slip agent composites with different aging times were investigated using polarized optical microscopy (POM, S38, Bimience).

Results and discussion

Surface morphology of PP/Slip agent composite

The samples before and after thermal aging were subjected to morphological analysis using a digital

camera. Figure 2 displays the close-up digital images of the PP/slip agent composites subjected to different slip agents and thermal aging times. In the composites aged 24–72 h (Fig. 2a–b), many migration-related whitenings were observed at the aging time of 24 h, and surface evaporation-based migration in the PP/amide composites (Fig. 2a) decreased at an aging temperature of 90 °C and an aging time of 72 h because of the high flowability of the amide nanoadditive. Conversely, significantly less migration was observed for the first 24 h of aging in the PP/Si compared with the PP/amide composites. Over time, more migration-related whitening was observed on the surface of the PP/Si composites. This result indicated that in the PP/amide composites, rapid migration occurred after 24 h up to 72 h of aging, compared with that in the PP/Si composites. Thus, it can be concluded that the migration process occurring in the PP/Si composites was slightly more stable than that which occurred in the PP/amide composites. The reason for the slower migration of the PP/Si composites was attributed to the fact that they had more functional oxygen groups than amides. Thus, it is estimated that compatibility with PP is higher. This surface migration phenomenon was believed to push the nanoadditives to the surface as the polymer chains moved, and as the polypropylene crystal structure changed owing to thermal aging. These changes can be confirmed by analyzing the crystallinity of the inner and outer parts of the PP composites.

Characterization of PP/Slip agent composite

Figure 3a,b shows the XPS atomic ratios of the PP/slip agent composites aged at 90 °C for 0–72 h. The XPS patterns of all samples exhibited a tendency to increase in the O/C, ratio calculated from the total content of O1s and C1s, atomic ratio after thermal aging, which was attributed to the whitening phenomenon of the amide and Si slip agents that migrated onto the PP/slip agent composite surface. Notably, in the PP/amide slip agent composite, the O/C atomic ratio decreased after 72 h of thermal aging. The amide slip agent added to the PP composites completely migrated to the surface after 48 h and then evaporated. It is considered that this effect reduced the O/C atomic ratio. From the results of the O/C atomic ratio, it was confirmed that the PP/Si slip agent composites had more stable migration
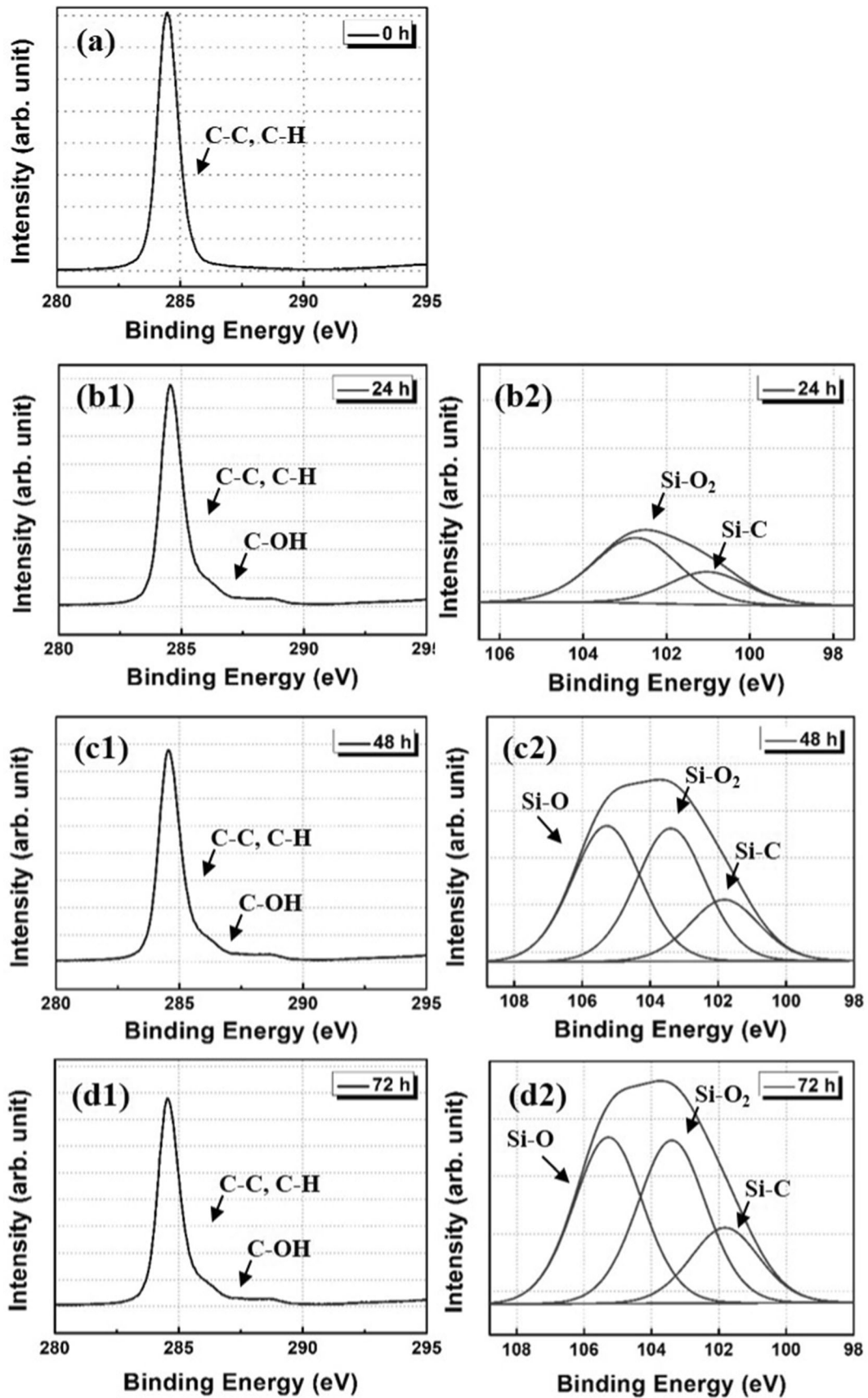
◄ **Figure 5** XPS C_{1s} and Si_{2p} spectra of PP/Si composites aged at 90 °C at different times. **a** C_{1s} spectra, aging time: 0 h, **b** C_{1s} and Si_{2p} spectra, aging time: 24 h, **c** C_{1s} and Si_{2p} spectra, aging time: 48 h, and **d** C_{1s} and Si_{2p} spectra, aging time: 72 h.

patterns than the PP/amide slip agent composites. The C_{1s}, N_{1s}, and Si_{2p} spectra of the PP/slip agent composites after thermal aging are shown in Figs. 4 and 5. The spectra show peaks attributed to C in the range 285–287 eV, N at 399.7 eV, and Si in the range 101–105 eV assigned to the C–C, C-H, C–OH, C=O, N–(C=O), Si–O, Si–C, and Si–O_2 groups, respectively, of the surface-migrated slip agents. Nanoadditive-related (amide and Si) peaks were not detected in the nonaged sample with the amide slip agent. In the case of amide, it was confirmed that the migration started at 0 h from the detection result of an O/C atomic ratio of 0.007. In contrast, no O/C atomic ratio was detected at 0 h for the sample containing the Si slip agent. The XPS surface elemental analysis results

for the PP/slip agent composites are listed in Table S1. From the results obtained from surface element analyses, in the case of PP composites, which contained amide, the N/C atomic ratio increased to 0.024 by 48 h and then decreased to 0.013 at 72 h. The amide additive was considered to be present inside the PP composites; they evaporated after they were transferred to the surface when exposed to thermal aging for a long time. By contrast, in the PP composites, which contained Si, the Si/C atomic ratio was detected as low as 0.005 at 24 h, and unlike PP/composites with amide, it did not evaporate and increased linearly until 72 h. These results show that the Si additive exhibits higher stability than the amide additive in accelerated aging conditions at 90 °C for 72 h.

A series of crystallization analyses involving thermal aging of the external and internal PP/slip agent composites were conducted at 90 °C for 0, 24, 48, and 72 h. The crystallization characteristics of the external and internal regions varied as a function of thermal
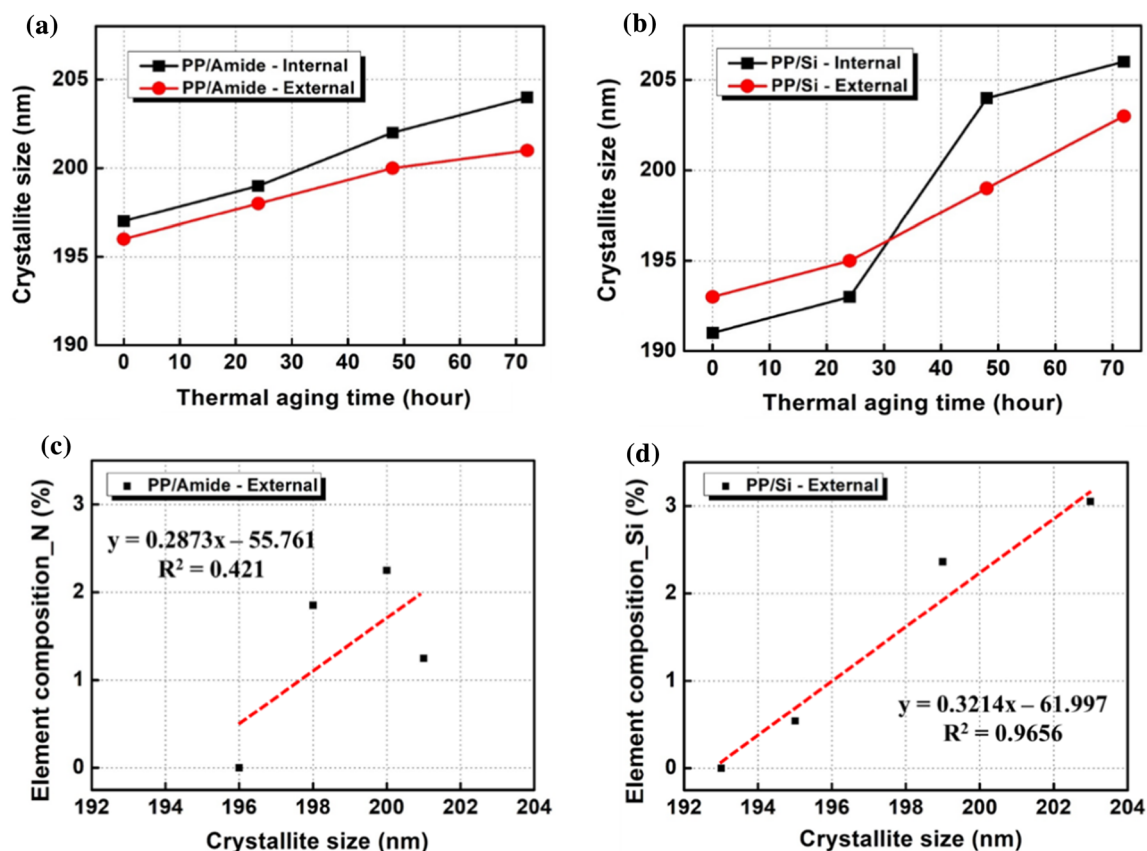

Figure 6 Variations in the crystallite size of **a** PP/amide composites; **b** PP/Si composites with the thermal aging time, as determined from the XRD data. Relationship between elemental composition and crystallite size of **c** PP/amide composites; **d** PP/Si composites aged at 90 °C at different times (0–72 h).

aging time. The XRD profiles shown in Fig. 3c–f reveal the aging time-dependent changes in the intensities of the diffraction peaks corresponding to the internal and external regions of the PP/slip agent composites thermally aged at 90 °C. The XRD experiments could not confirm the quantitative measurement of the nanoadditive migration. However, it was assumed that the talc peak intensity was proportional to the amount of nanoadditive that migrated at 0, 24, 48, and 72 h of thermal aging. It is evident from Fig. 3c–f that the nanoadditive migrated to the surfaces of the samples from the internal regions upon annealing, as revealed by the corresponding increase in the intensity of the nanoadditive peak. In addition, the results show an increase in the mass concentration of the nanoadditive phase on the surface of the samples with aging time. This indicates that migration was significantly affected by the thermal aging time. In addition, the XRD pattern in Fig. 3c–f shows the presence of basal diffraction of talc (T) (001), (002), (003), and (020) in the PP/slip agent composites, and the internal intensity decreases with increasing thermal aging time. Simultaneously, the external intensity increased.

Figure 6a–b shows the correlation between the slip agent migration and nanocrystallite size in the thermally treated PP/slip agent composites. The correlation was evidenced by the increase in the spherulite size (nm), as measured by XRD at different aging periods. Because the samples were thermally aged at temperatures below their melting temperatures, the crystallite size eventually increased. This caused the migration of low molecular weight nanoadditives to the sample surface. In composite samples, low molecular weight nanoadditives are usually present in the amorphous regions of the polymer. However, thermal aging changes the amorphous fractions, and the segments of the mobile regions entangle with each other, leading to restricted motion, such as in secondary crystallization during annealing [37, 38]. The entangling of the chains within the adjacent crystals causes thickening of the lamellae and increases the crystallite size during the annealing process. The sizes of the crystallites in the melted compound in the external and internal regions were different. This finding can be attributed to thermal hysteresis during injection molding. In addition, it is possible that the effect of thermal aging manifested as an increase in the crystalline particle size owing to the effect of the remaining lamellar or crystalline chains.

In polymers, the crystallite size is influenced by the type of nucleating agent, temperature, thermal characteristics, and velocity gradient of the polymer. Rapid quenching produces numerous nuclei simultaneously, thus resulting in a small grain size. However, after the initial nucleus is formed, the grain size may change slightly with thermal aging. In this study, it was confirmed that the thermal aging treatment caused an increase in the crystallite size. As a result, the nanoadditive present in the amorphous regions diffused to the periphery. Therefore, the increase in the crystallite size was attributed to the migration of the nanoadditive to the surface owing to annealing. The calculated FWHM values and crystallite sizes are listed in Tables S2 and S3. However, it should be noted that only the parameters of PP in XRD were considered, except for the parameters of talc. Given that talc is an inorganic material, it exhibits high-intensity peaks. Therefore, we need to distinguish the talc peaks from the PP peaks.

A comparison of the XPS analysis results of the PP/slip agent composites with less nanoadditive migration with that of the sample with more nanoadditive migration (Figs. 4 and 5) showed that thermal aging conditions accelerated the increase in the crystallite size of the PP composites, which resulted in a reduction in the average amorphous parts. This shows that the nanoadditive, which comprises amorphous components and is present in the amorphous portions, migrated to the sample surface over time. Therefore, the XPS results indicated an increase in the amount of the nanoadditive migrated at different conditions during the thermal treatment. Figure 6c–d shows the linear relationship of element composition and crystallite size. This confirmed that the nanocrystallite size increase was proportional to the nanoadditive content, as indicated by the XPS results.

The DSC thermograms corresponding to the external and internal regions of the PP/slip agent composites thermally aged for different times are shown in Fig. 7a–d. The melting endotherms show changes related to the increase in the crystallite size of the samples induced by thermal aging. As observed in Fig. 6a–b, the average size of the crystals increased with thermal aging for 0, 24, 48, and 72 h, which is attributed to the formation of thinner lamellar stacks owing to the crystallization of the remaining mobile lamellae between the primary stacks [39]. Earlier studies on crystallization have led
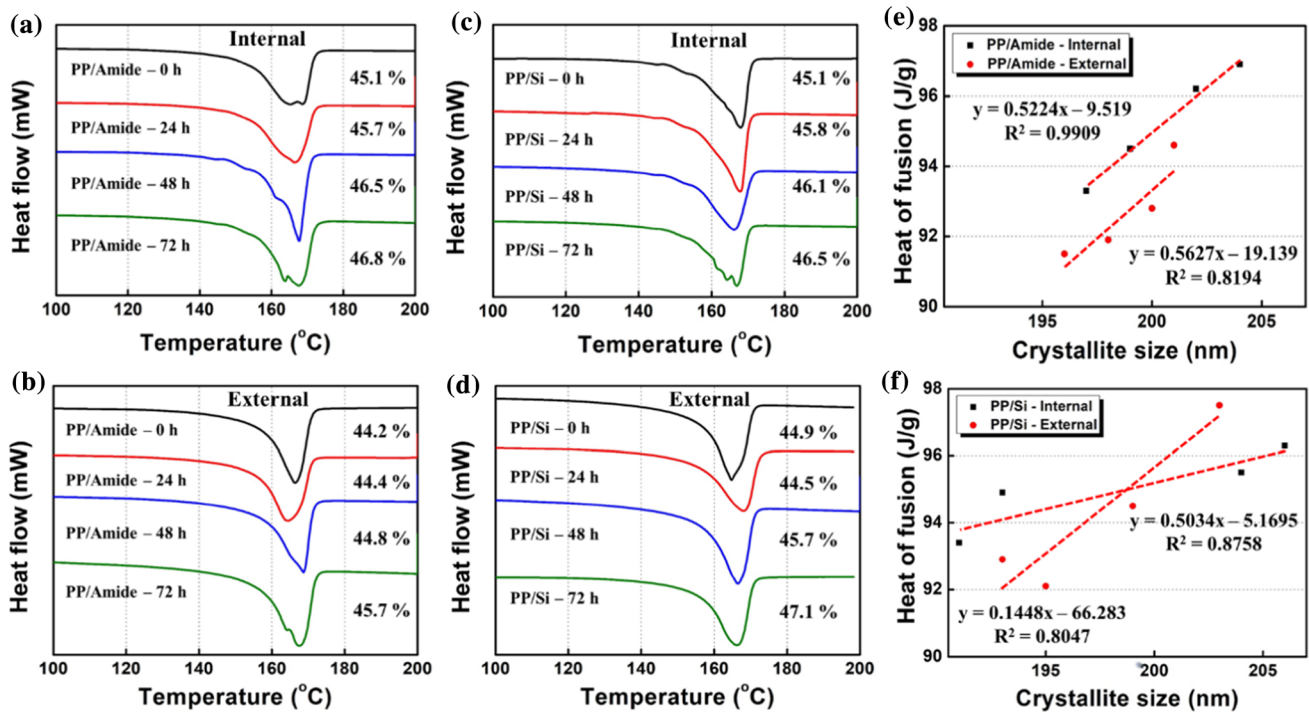
Figure 7 Differential scanning calorimeter (DSC) thermograms corresponding to **a** internal and **b** external regions of PP/amide composites aged at 90 °C for different times. **c** Internal and **b** external regions of PP/Si composites aged 90 °C for different times. Relationship between heat of fusion (J/g) and crystallite size (nm) of **e** PP/amide composites and **f** PP/Si composites aged at 90 °C for different times (0–72 h).

to the conclusion that rearrangement, such as secondary crystallization of semicrystalline polymers, could be related to the changes in the crystalline and amorphous parts of the samples with thermal aging. The lament amorphous regions have a particular mobility, which implies restricted motion owing to the entanglement of lamellar stacks in the intercrystalline regions. Hence, a slight increase in the heat of fusion of the samples was observed at different thermal conditions, as shown in Fig. 7a–d. These changes are considered evidence of the heat of fusion of the samples at different thermal conditions.

This increase in the heat of fusion is a direct indication of the crystallinity of the samples. Figure 7e–f shows a linear relationship between the heat of fusion and crystallite size of the samples thermally aged at 90 °C for 0, 24, 48, and 72 h. A universal method for measuring the degree of crystallization can be obtained by integrating the area under the endotherm and by dividing it by the heat of fusion of 100% crystalline PP ($\Delta H_{100\%} \approx 207$ J/g).

Table S4 lists the DSC results, including the melting peak temperature (T_m), crystallization peak temperature (T_c), heat of fusion (ΔH_m), and degree of crystallinity (X_c). Notably, the thermal aging of the samples at 90 °C did not significantly affect the T_m and T_c. Moreover, with aging time, the heat of fusion and degree of crystallinity changed slightly. This was attributed to the modifications of the crystalline and amorphous regions without any structural changes.

Therefore, the results implied that the increase in the melting enthalpy was related to the increase in crystallite size and the reduction of amorphous fractions in the sample. It was demonstrated that an amorphous component, such as slip agents, with limited solubility in the matrix migrates and coagulates at the sample surface, thus affecting the appearance of the final product and reducing the function of the slip agents. A schematic of the proposed mechanism of crystallization–migration occurring in the PP/slip agent composites subjected to accelerated aging is shown in Fig. 8. The crystallization behavior, crystallization size increase, melting enthalpy, and the proposed crystallization–migration mechanism were investigated through EDS mapping. As shown in Figs. 9 and 10, which are SEM/EDS mapping of PP/slip agent composites, amide and Si were partially found on the external

Figure 8 Schematic of mechanism of crystallization–migration in PP/slip agent composites subjected to accelerated aging.
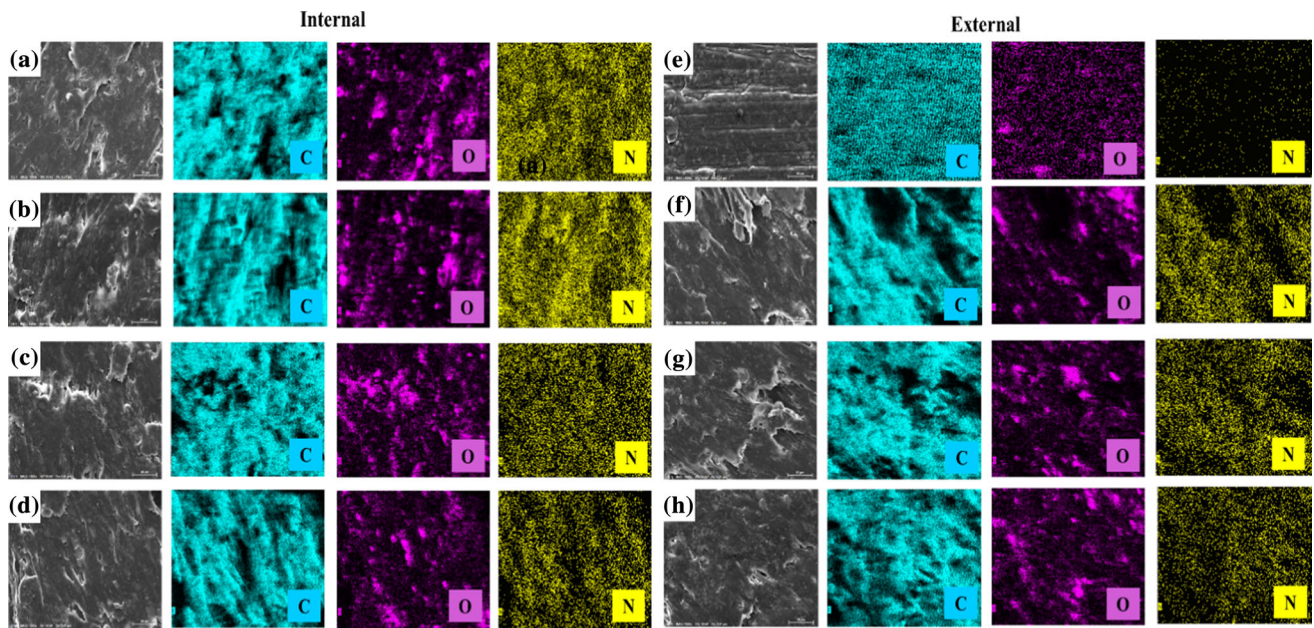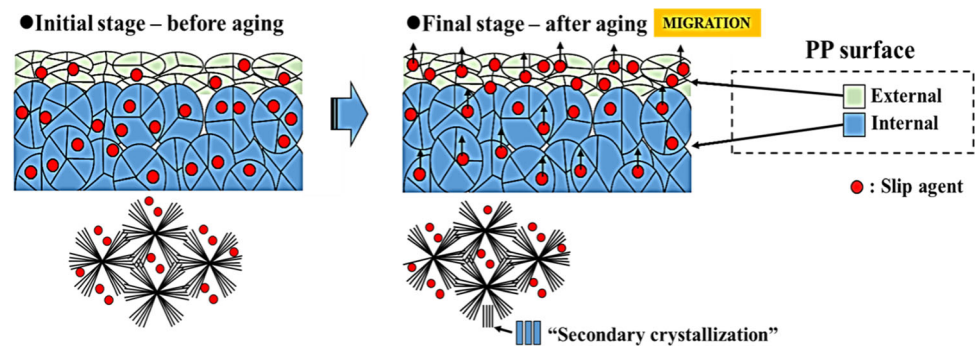

Figure 9 FESEM/EDS mapping showing the distribution of carbon (C), oxygen (O), and nitrogen (N) on the PP/amide composites aged at 90 °C for different times. **a** 0 h, **b** 24 h, **c** 8 h, **d** 72 h of internal, **e** 0 h, **f** 24 h, **g** 48 h, **h** 72 h of external.

surface of the PP/slip agent composites at an aging time of 0 h, but a significant amount was observed as the aging time increased. These results insist that the nanoadditive migrates to the outside due to the increased crystallite size by changes in crystallinity and heat of fusion. This also demonstrates the mechanism of crystallization–migration in Fig. 8.

Many parameters can be used to evaluate the scratch performance of polymeric materials. Different methods, such as the ASTM/ISO method, which is based on the critical load level at the onset of scratch visibility, and the Erichsen method, which is based on the difference in brightness of the sample surface before and after the scratch test, named lightness (L*), are used to evaluate the material scratch performance. The worse the scratch resistance of the material is, the larger the value of L*. Although there

is no straightforward correlation between these two parameters, the value of L* is considered a good qualitative index for evaluating the scratch resistance under a certain load level. In addition, the scratch resistance denotes the ability of a material to withstand abrasive interactions with another body. This is not the same as the abrasion resistance and wear commonly addressed in the literature. A scratch was created when the material was subjected to an indentation force. When a scratch is developed, an uneven surface results in nonuniform light scattering and "scratch whitening," especially for filled materials.

Figure 11a–d shows the variation in L* of the PP/slip agent composites with aging time and the correlation between L* and the surface roughness, respectively. As observed, for the sample with the Si
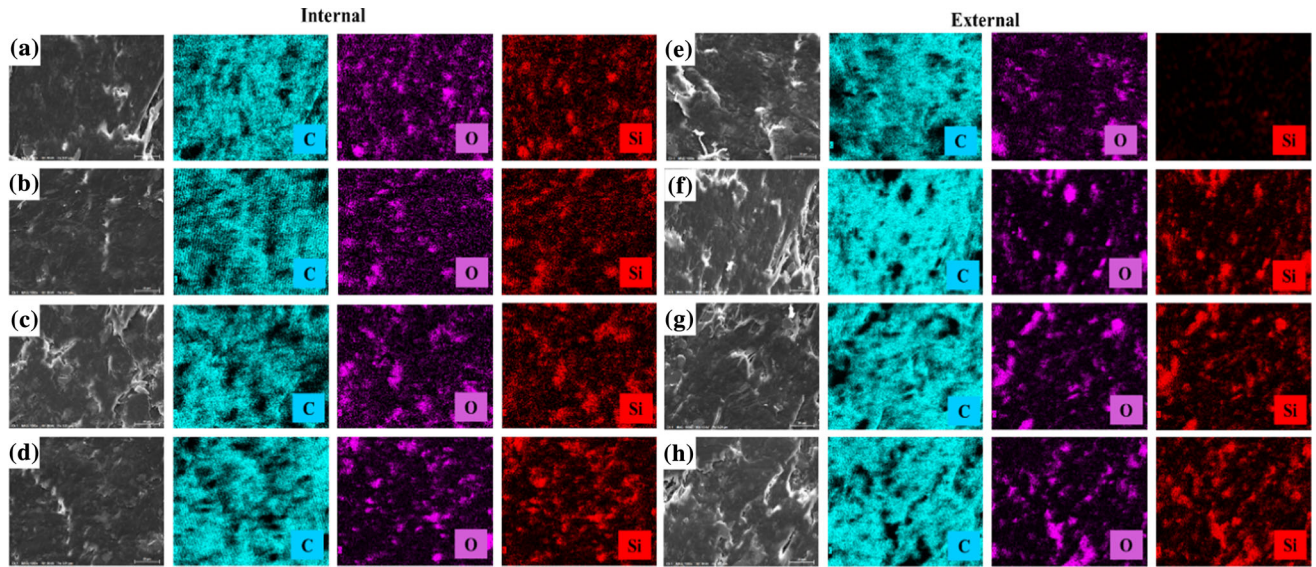
Figure 10 FESEM/EDS mapping showing the distribution of carbon (C), oxygen (O), and silicon (Si) on the PP/Si composites aged at 90 °C for different times. **a** 0 h, **b** 24 h, **c** 48 h, **d** 72 h of internal, **e** 0 h, **f** 24 h, **g** 48 h, **h** 72 h of external.
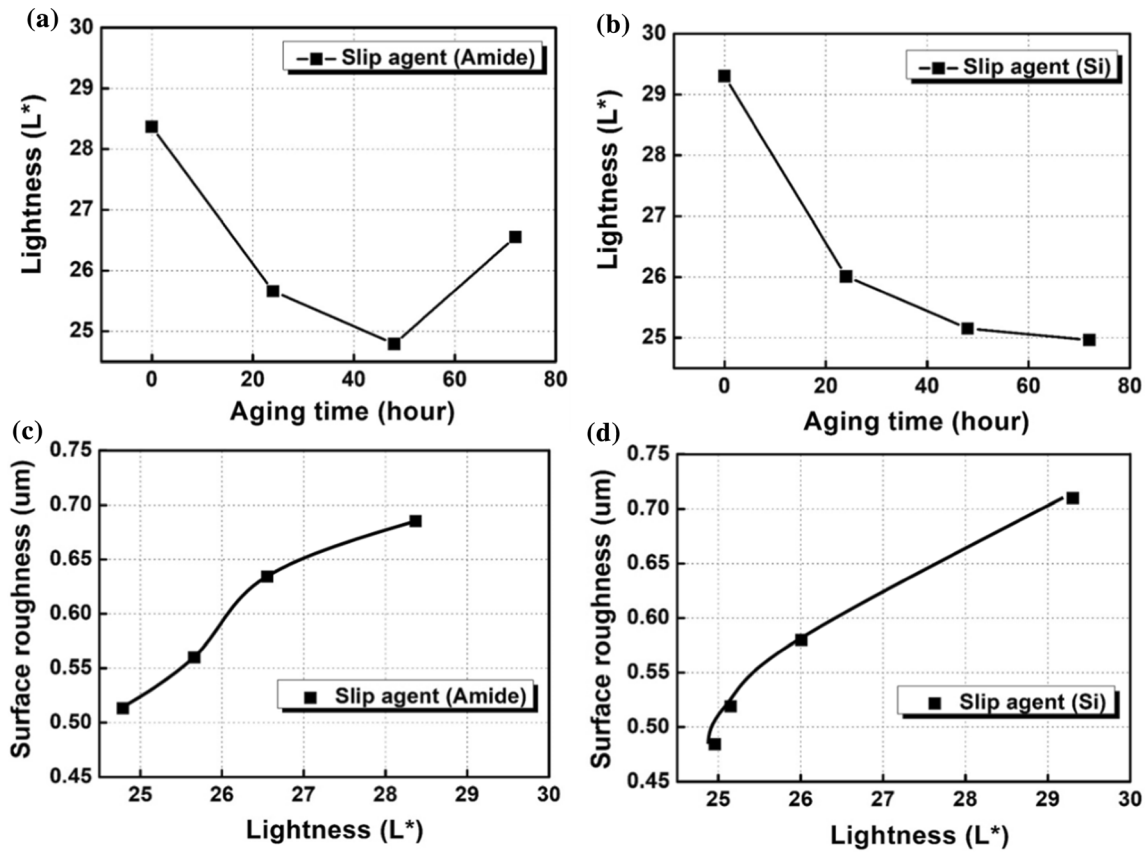

Figure 11 Variation in L* and simulated area fraction of **a** PP/amide composites and **b** PP/Si composites with aging time. Correlation between L* and surface roughness of the aged **c** PP/amide composites and **d** PP/Si composites.
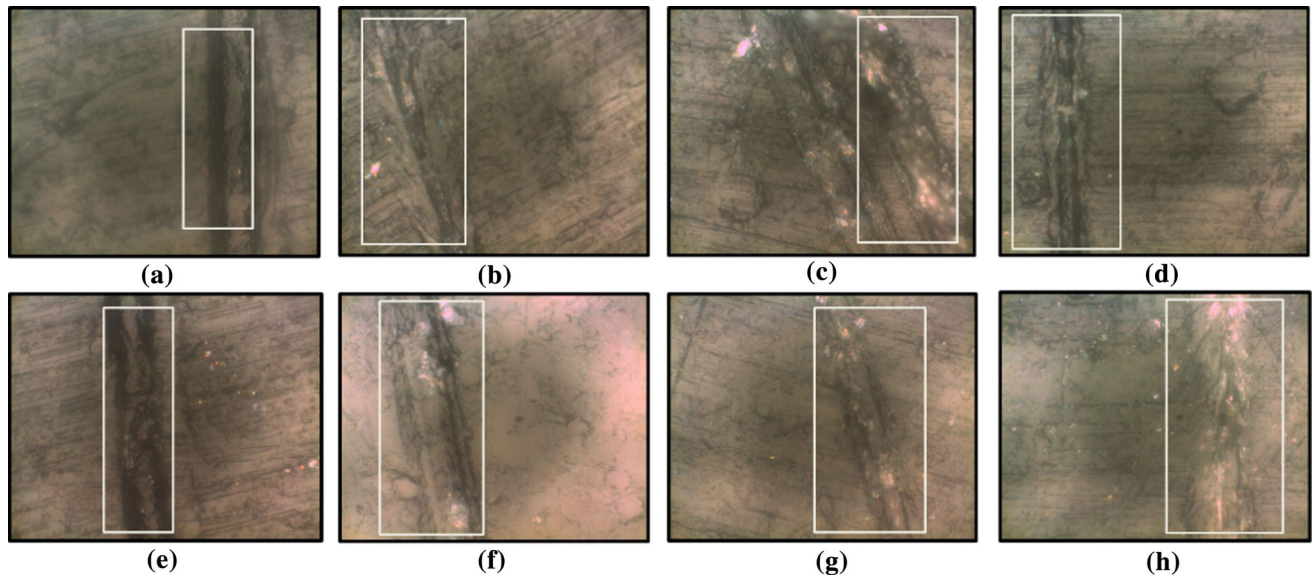
Figure 12 Optical microscope images of PP/amide composites aged at 90 °C with **a** 0 h, **b** 24 h, **c** 48 h, **d** 72 h and PP/Si composites aged at 90 °C with **e** 0 h, **f** 24 h, **g** 48 h, **h** 72 h.

slip agent, the L* value decreased with aging time because of the migration of the slip agent to the surface. However, for the sample with the amide slip agent, the L* value continually decreased up to 48 h of aging, after which it increased owing to the evaporation of the slip agents (Fig. 11a–b). At the same level of normal scratch load, the L* value increased with the broadening of the surface roughness (Fig. 11c–d). When the scratch tip moves on a material with poor scratch resistance, the tangential force between the tip and the substrate produces severe deformation/damage. Figure 12 shows an optical microscope image of the surface after scratching. Scratch whitening was not observed for both PP/amide composites and PP/Si composites at an aging time of 0 h; however, as shown in the correlation between L* and the surface roughness in Fig. 11, scratch whitening was observed as the slip agent migrated on the surface by aging time.

Conclusions

In this study, the characteristics of slip agent migration on the surfaces of PP/slip agent composites subjected to accelerated aging were investigated, and the following conclusions were drawn.

1. The increase in the average crystallite size was attributed to the migration of slip agents owing to thermal aging for 0–72 h. Accelerated thermal aging caused an increase in the size of the crystallites in the external and internal regions of the composites. Consequently, the relationship between the crystallite size and the extent of migration of the slip agent on the surfaces of the PP/slip agent composites was found to be linear.

2. The increase in the heat of fusion was a direct indication of thicker lamellae and higher crystallinity. An increase in the heat of fusion with an increase in the thermal aging time leads to the formation of "secondary lamellae" with an increase in the thermal aging time. In addition, the extent of migration was proportional to the melting enthalpy and crystallite size of the PP/slip agent composites during accelerated aging.

3. As observed from the lightness and surface roughness analysis data, the L* value decreased with aging time because of the migration of the slip agent to the sample surface. For the sample with the amide slip agent, the L* value first decreased and then increased (after 48 h) because of the evaporation of the slip agent. At the same level of normal scratch load, the L* value increased with the broadening of the surface roughness.

4. Close-up images, XPS profiles, and SEM/EDS mapping images of the PP/slip agent composites aged at 90 °C for different times (0–72 h) revealed the presence of slip agents on the surfaces of the

composites; notably, the amide slip agent migrated within a short period. In addition, in the composites, the migration of the Si slip agent was found to be more stable and slower than that of the amide slip agent.

Acknowledgements

Data availability

The raw/processed data required to reproduce these findings cannot be shared at this time as the data also form part of an ongoing study.

Declarations

Conflict of interest The authors declare that they have no known competing financial interests or personal relationships that could have appeared to influence the work reported in this paper.

Supplementary Information: The online version contains supplementary material available at https://doi.org/10.1007/s10853-021-06694-4.

References

[1] Martial F, Huguet J, Bunel C (1999) Development of a quantitative analysis method for polypropylene additives using on-line SFE/SFC. Polym Int 48:299–306. https://doi.org/10.1002/(SICI)1097-0126(199904)48:4%3c299::AID-PI148%3e3.0.CO;2-5

[2] Bak M-G, Won J-S, Koo S-W, Oh A, Lee H-K, Kim D-S et al (2021) Migration behavior of lubricants in polypropylene composites under accelerated thermal aging. Polymers 13(11):1723. https://doi.org/10.3390/polym13111723

[3] Arencón D, Velasco JI, Realinho V, Sánchez-Soto M, Gordillo A (2007) Fracture toughness of glass microsphere-filled polypropylene and polypropylene/poly (ethylene terephthalate-co-isophthalate) blend-matrix composites. J Mater Sci 42:19–29. https://doi.org/10.1007/s10853-006-1036-1

[4] El Mansouri H, Yagoubi N, Ferrier D (1998) Extraction of polypropylene additives and their analysis by HPLC. Chromatographia 48:491. https://doi.org/10.1007/BF02466639

[5] Shuler CA, Janorkar AV, Hirt DE (2004) Fate of erucamide in polyolefin films at elevated temperature. Polym Eng Sci 44:2247–2253. https://doi.org/10.1002/pen.20252

[6] Llop C, Manrique A, Navarro R, Mijangos C, Reinecke H (2011) Control of the migration behavior of slip agents in polyolefin-based films. Polym Eng Sci 51:1763–1769. https://doi.org/10.1002/pen.21963

[7] Mohmeyer N, Behrendt N, Zhang X, Smith P, Altstädt V, Sessler GM et al (2007) Additives to improve the electret properties of isotactic polypropylene. Polymer 48:1612–1619. https://doi.org/10.1016/j.polymer.2006.08.001

[8] Bigger SW, O'Connor MJ, Scheirs J, Janssens JLGM, Linssen JPH, Legger-Huysman A (1996) Odor characterization of low-density polyethylene used for food-contact applications. Polym Durab 249:249–268. https://doi.org/10.1021/ba-1996-0249.ch017

[9] Garrido-López Á, Esquiu V, Tena MT (2006) Determination of oleamide and erucamide in polyethylene films by pressurised fluid extraction and gas chromatography. J Chromatogr A 1124:51–56. https://doi.org/10.1016/j.chroma.2006.04.086

[10] Jiang H, Cheng Q, Jiang C, Zhang J, Yonghua L (2015) Effect of stick-slip on the scratch performance of polypropylene. Tribol Int 91:1–5. https://doi.org/10.1016/j.triboint.2015.06.024

[11] Wakabayashi M, Kohno T, Tanaka Y, Kanai T (2009) Study on the bleeding mechanism of slip agents in a polypropylene film using molecular dynamics. Int Polym Process INT POLYM PROC 24:133–140. https://doi.org/10.3139/217.2211

[12] Xu WC, Li DL, Fu YB, Shang W (2013) A modified polypropylene resin for food packaging. Adv Mater Res 631–632:598–602.

[13] Kismet Y, Wagner MH (2018) Mechanical and flow properties of blends of polypropylene and powder coating recyclates with and without addition of maleic anhydride. Adv Polym Technol 37:3511–3518. https://doi.org/10.1002/adv.22135

[14] Schöne J, Kotter I, Grellmann W (2012) Properties of polypropylene talc compounds with different talc particle size and loading. Zeitschrift Kunststofftechnik/J Plastics Technol 8:230–251

[15] Tadele D, Roy P, Defersha F, Misra M, Mohanty AK (2020) A comparative life-cycle assessment of talc- and biochar-reinforced composites for lightweight automotive parts. Clean Technol Environ Policy 22:639–649. https://doi.org/10.1007/s10098-019-01807-9

[16] Fujiyama M, Wakino T (1991) Crystal orientation in injection molding of talc-filled polypropylene. J Appl Polym Sci 42:9–20. https://doi.org/10.1002/app.1991.070420103

[17] Spatafore R, Pearson LT (1991) Migration and blooming of stabilizing antioxidants in polypropylene. Polym Eng Sci 31:1610–1617. https://doi.org/10.1002/pen.760312209

[18] Spatafore R, Schultz K, Thompson T, Pearson LT (1992) Migratory behaviour of a phosphite process stabilizer in polyolefins. Polym Bull 28:467–472. https://doi.org/10.1007/BF00297341

[19] Nouman M, Saunier J, Jubeli E, Yagoubi N (2017) Additive blooming in polymer materials: consequences in the pharmaceutical and medical field. Polym Degrad Stab 143:239–252. https://doi.org/10.1016/j.polymdegradstab.2017.07.021

[20] Ferhoum R, Ould OM (2013) Analysis of thermal ageing effect (hold time - crystallinity rate - mechanical property) on high density polyethylene (HDPE). Int J Mater Sci Appl 2:109. https://doi.org/10.11648/j.ijmsa.20130203.17

[21] Dudić D, Kostoski D, Djoković V, Stojanović Z (2000) Recrystallization processes induced by accelerated ageing in isotactic polypropylene of different morphologies. Polym Degrad Stab 67:233–237. https://doi.org/10.1016/S0141-3910(99)00118-4

[22] Natale R, Russo R, Vittoria V (1992) Crystallinity of isotactic polypropylene films annealed from the quenched state. J Mater Sci 27:4350–4354. https://doi.org/10.1007/BF00541565

[23] Oreski G, Wallner GM (2009) Evaluation of the aging behavior of ethylene copolymer films for solar applications under accelerated weathering conditions. Sol Energy 83:1040–1047. https://doi.org/10.1016/j.solener.2009.01.009

[24] Shen Y, Yang D, Feng Z (1991) Epitaxial crystallization of high-density polyethylene on polypropylene in solution-cast films. J Mater Sci 26:1941–1946. https://doi.org/10.1007/BF00543627

[25] Law A, Simon L, Lee-Sullivan P (2008) Effects of thermal aging on isotactic polypropylene crystallinity. Polym Eng Sci 48:627–633. https://doi.org/10.1002/pen.20987

[26] Kloziński A, Jakubowska P (2019) The effect of the addition of a slip agent on the rheological properties of polyethylene: off-line and in-line measurements. J Polym Eng 39:422–431. https://doi.org/10.1515/polyeng-2018-0199

[27] O'Brien A, Cooper L (2001) Polymer additive migration to foods—a direct comparison of experimental data and values calculated from migration models for polypropylene. Food Addit Contam 18:343–355. https://doi.org/10.1080/02652030116702

[28] Kirchkeszner C, Petrovics N, Tábi T, Magyar N, Kovács J, Szabó BS et al (2022) Swelling as a promoter of migration of plastic additives in the interaction of fatty food simulants with polylactic acid- and polypropylene-based plastics. Food Control 132:108354. https://doi.org/10.1016/j.foodcont.2021.108354

[29] Song YS, Koontz JL, Juskelis RO, Patazca E, Limm W, Zhao K (2021) Effect of high pressure processing on migration characteristics of polypropylene used in food contact materials. Food Addit Contam Part A 38(3):513–531. https://doi.org/10.1080/19440049.2020.1861341

[30] Fasihnia SH, Peighambardoust SH, Peighambardoust SJ, Oromiehie A, Soltanzadeh M, Peressini D (2020) Migration analysis, antioxidant, and mechanical characterization of polypropylene-based active food packaging films loaded with BHA, BHT, and TBHQ. J Food Sci 85:2317–2328. https://doi.org/10.1111/1750-3841.15337

[31] Monshi A, Foroughi MR, Monshi M (2012) Modified scherrer equation to estimate more accurately nano-crystallite size using XRD. World J Nano Sci Eng 2:154–160. https://doi.org/10.4236/wjnse.2012.23020

[32] Bokuniaeva AO, Vorokh AS (2019) Estimation of particle size using the Debye equation and the Scherrer formula for polyphasic TiO2 powder. J Phys: Conf Ser 1410:012057. https://doi.org/10.1088/1742-6596/1410/1/012057

[33] Muniz FTL, Miranda MAR, Morilla dos Santos C, Sasaki JM (2016) The Scherrer equation and the dynamical theory of X-ray diffraction. Acta Crystallogr Sect A 72:385–390. https://doi.org/10.1107/S205327331600365X

[34] Chukhchin DG, Malkov AV, Tyshkunova IV, Mayer LV, Novozhilov EV (2016) Diffractometric method for determining the degree of crystallinity of materials. Crystallogr Rep 61:371–375. https://doi.org/10.1134/S1063774516030081

[35] Arvidson SA, Khan SA, Gorga RE (2010) Mesomorphic−α-monoclinic phase transition in isotactic polypropylene: a study of processing effects on structure and mechanical properties. Macromolecules 43:2916–2924. https://doi.org/10.1021/ma1001645

[36] Asiltürk İ, Çunkaş M (2011) Modeling and prediction of surface roughness in turning operations using artificial neural network and multiple regression method. Expert Syst Appl 38:5826–5832. https://doi.org/10.1016/j.eswa.2010.11.041

[37] Wang W, Zhao G, Wu X, Zhai Z (2015) The effect of high temperature annealing process on crystallization process of polypropylene, mechanical properties, and surface quality of plastic parts. J Appl Polymer Sci 132(46):42773. https://doi.org/10.1002/app.42773

[38] Ahmed AK, Atiqullah M, Pradhan DR, Al-Harthi MA (2017) Crystallization and melting behavior of i-PP: a perspective from Flory's thermodynamic equilibrium theory and

DSC experiment. RSC Adv 7:42491–42504. https://doi.org/10.1039/C7RA06845J

[39] Ezquerra TA, Šics I, Nogales A, Denchev Z, Baltá-Calleja FJ (2002) Simultaneous crystalline-amorphous phase evolution during crystallization of polymer systems. EPL (Europhys Lett) 59:417